Electronic Structural Information from Q-Band ENDOR on the Type 1 and Type 2 Copper Liganding Environment in Wild-Type and Mutant Forms of Copper-Containing Nitrite Reductase†

Andrei Veselov,‡ Kenneth Olesen,§,|| Andrzej Sienkiewicz,‡,⊥ James P. Shapleigh,§ and Charles P. Scholes*,‡

Department of Chemistry, Center for Biophysics and Biochemistry, University at Albany, SUNY, Albany, New York 12222, and Department of Microbiology, Wing Hall, Cornell University, Ithaca, New York 14853

Received July 2, 1997; Revised Manuscript Received February 3, 1998

ABSTRACT: Q-band ENDOR elucidated proton and nitrogen hyperfine features to provide spin density information at ligands of blue-green Type 1 and catalytic Type 2 copper centers in nitrite reductase. The blue-green Type 1 center of nitrite reductase has a redox, electron-transfer role, and compared to the blue center of plastocyanin, it has the following structural differences: a shortened $Cu-S_{met}$ bond length, a longer $Cu-S_{cys}$ bond length, and altered ligand−copper−ligand bond angles (Adman, E. T., Godden, J. W., and Turley, S. (1995) *J. Biol. Chem. 270*, 27458−27474). The hyperfine couplings of the two Type 1 histidine (N_δ) ligands showed a larger percentage difference from each other in electron spin density than previously reported for other blue Type 1 proteins, while the cysteine β-proton hyperfine couplings, a measure of unpaired pπ spin density on the liganding cysteine sulfur, showed a smaller electron spin density. A mutation of the Type 1 center, M182T, having the copper-liganding Met^{182} transformed to Thr^{182}, caused the center to revert to an optically "blue" center, raised its redox potential by ∼100 mV, and led to the loss of activity (prior paper). Surprisingly, in M182T there was *no change* from native Type 1 copper either in the histidine or cysteine hyperfine couplings or in *g* values and Cu nuclear hyperfine couplings. The conclusion is that the optical and redox alterations due to changed Type 1 methionine ligation need not be concurrent with electron spin delocalization changes in the HOMO as reported from its essential cysteine and histidines. A detailed picture of the nitrogen couplings from the three histidine (N_ϵ) ligands of the Type 2 center indicated a substantial (∼200%) electronic hyperfine inequivalence of one of the histidine nitrogens from the other two within the Type 2 HOMO and thus provided evidence for electronic distortion of the Type 2 site. In the presence of the nitrite substrate, hyperfine couplings of all histidines diminished. We suggest that this nitrite-induced decreased covalency would correlate with an increased Type 2 redox potential to assist electron transfer to the Type 2 center. Dipole-coupled, angle-selected exchangeable proton features, observed over a range of *g* values, predicted a ligand−water proton distance of 2.80 Å from copper, and these water protons were eliminated by nitrite. His^{287} is not a Type 2 ligand but is positioned to perturb an axial water or a nitrite of Type 2 copper. In the presence of nitrite the mutant H287E showed no evidence for the loss of water protons and no diminished ligand histidine covalency. H287E has vastly diminished activity (prior paper), and the ENDOR information is that NO_2^- does not bind to Type 2 copper of H287E. In summary, the electronic information from this study of native and suitably chosen mutants provided a test of the highest occupied molecular orbital (HOMO) wave function at Type 1 and Type 2 coppers and an intimate electronic insight into functional enzymatic properties.

INTRODUCTION

Nitrite reductase (Nir)[1] catalyzes the reduction of nitrite to nitric oxide:

$$NO_2^- + 2H^+ + e^- \rightarrow NO + H_2O$$

The enzyme used for this study is a component of the bacterial denitrification pathway which converts nitrate to nitrogen gas ($NO_3^- \rightarrow \mathbf{NO_2^-} \rightarrow \mathbf{NO} \rightarrow N_2O \rightarrow N_2$). As

† These studies were partially supported by the NIH (GM-35103, C.P.S.), the USDA (J.P.S.), and the Maria Sklodowska Curie US−Polish Joint Fund II, PAN/NIST-94-203 (A.S.).

* To whom correspondence should be addressed. Phone: 518-442-4551. Fax: 518-442-3462. E-mail: cps14@cnsvax.albany.edu.

‡ University at Albany.

§ Cornell University.

|| Present address: Department of Biochemistry and Biophysics, Lundberg Institute, Göteborg University and Chalmers University of Technology, Medicinaregatan 9C, S-413 90, Göteborg, Sweden.

⊥ Present address: Institute of Physics of the Polish Academy of Sciences, Al. Lotnikow 32/46, 02-668, Warsaw, Poland.

[1] Abbreviations and definitions: RF, radio frequency; ptp, peak-to-peak; G, gauss; kG, kilogauss; i.d., inside diameter; o.d., outside diameter; EPR, electron paramagnetic resonance; ENDOR, electron nuclear double resonance; ESEEM, electron spin−echo envelope modulation; Nir, nitrite reductase; M182T, a mutant form of Nir where the Met^{182} ligand at the Type 1 center was mutated to threonine; H287E, a mutant form of Nir where the His^{287} residue near, but not liganding, to the Type 2 center, was mutated to glutamic acid; TD, Nir depleted of Type 2 copper.

S0006-2960(97)01604-8 CCC: $15.00
Published on Web 04/04/1998

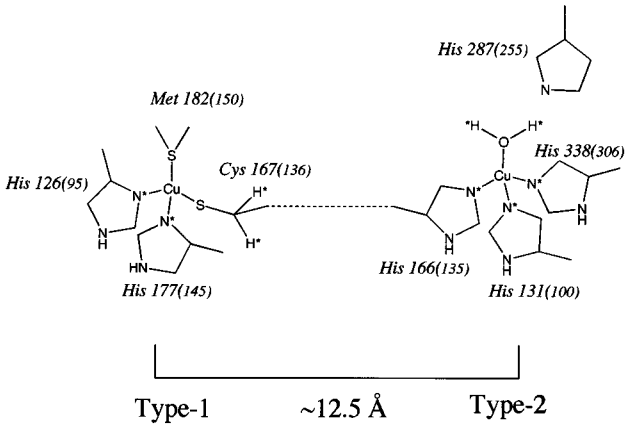

FIGURE 1: Schematic representation of the copper sites in nitrite reductase from Adman et al. (*2*). Starred nuclei (*) are those observed by ENDOR. The bond angles and bond distances were obtained from the average over three subunits from the pH 6.8 crystal data of Adman et al. (*2*). For Type 1: $S^{Met}-Cu-S^{Cys} = 105°$, $S^{Met}-Cu-N^{126} = 89°$, $S^{Met}-Cu-N^{177} = 133°$, $S^{Cys}-Cu-N^{126} = 136°$, $S^{Cys}-Cu-N^{177} = 105°$, $N^{126}-Cu-N^{177} = 100°$; $Cu-S^{Met} = 2.49$ Å, $Cu-S^{Cys} = 2.16$ Å, $Cu-N^{126} = 1.99$ Å, $Cu-N^{177} = 2.00$ Å. For Type 2: $OW-Cu-N^{131} = 108°$, $OW-Cu-N^{166} = 109°$, $OW-Cu-N^{338} = 119°$, $N^{131}-Cu-N^{166} = 107°$, $N^{131}-Cu-N^{338} = 99°$, $N^{166}-Cu-N^{338} = 114°$; $Cu-N^{131} = 1.99$ Å, $Cu-N^{166} = 2.01$ Å, $Cu-N^{338} = 2.00$ Å, $Cu-OW = 2.02$ Å.

detailed in the accompanying paper, our enzyme was obtained by overexpressing Nir from *Rhodobacter sphaeroides* 2.4.3 in *Escherichia coli*. This enzyme contains two different types of copper, a Type 1 blue-green center which has an electron transfer/redox function and a Type 2 catalytic center where the nitrite is reduced to NO. The X-ray crystallographic features of copper-containing Nir from *Achromobacter cycloclastes* (*1, 2*) and *Alcaligenes faecalis* (*3*) have been determined. There is great sequence homology among this family of proteins, and Nir from *R. sphaeroides* 2.4.3 has at least 60% identity with other known sequences (*4*). The homology suggests that there will also be significant conservation of the secondary and tertiary structure among this family of proteins.

In Figure 1 we show the local liganding environment of both Type 1 and Type 2 centers as taken from the *A. cycloclastes* work of Adman et al. (*2*). The large numbering in that figure is derived from the deduced primary sequence of our *R. sphaeroides* protein, and the numbers in parentheses are from the *A. cycloclastes* sequence. Relevant bond angles and bond distances from the X-ray structure of *A. cycloclastes* Nir (pH 6.8) (*2*) are given in the legend of Figure 1. The Type 1 center does have the typical His-His-Cys-Met local ligation of other blue proteins such as plastocyanin (*5*) and azurin (*6*). However, the Type 1 copper of Nir has the following structural differences from more widely studied blue proteins: a shortened $Cu-S_{met}$ bond length, a longer $Cu-S_{cys}$ bond length, and altered ligand−copper−ligand bond angles. Unlike blue plastocyanin, which has the major optical absorption near 600 nm, the optical spectrum of cupric Type 1 copper in Nir has approximately equal absorption maxima at both 453 and 585 nm that give it a distinguishing blue-green color. Spectroscopies that probe transitions to excited electronic states (*7*) have given evidence for electronic differences between Type 1 centers, and LaCroix et al. (7) combined spectroscopic investigations with density functional calculations to define what was called "the extremely 'perturbed' electronic structure of this site relative to that of the prototypical 'classic' site in plastocyanin". However, a direct way of probing the ground state electronic structure of the HOMO (highest occupied molecular orbital) in Type 1 copper sites is to measure its wave function dependent ligand hyperfine couplings, notably at histidine and cysteine. The HOMO of the Type 1 center is the one which contains the unpaired electron spin, has significant copper $d_{x^2-y^2}$ and cysteine sulfur character, and significantly partakes in redox behavior and electron transfer. Changes in the covalent overlap with the ligands of a spin-containing orbital translate into changes in ligand hyperfine couplings. Hyperfine couplings provide an experimental test of the HOMO wave function for the Nir Type 1 center such as predicted recently in ref 7. The technique of choice for studying hyperfine couplings is ENDOR, which has been applied elegantly to other blue proteins by Hoffman and co-workers (*8, 9*), and as result, ENDOR spectra of relevant histidine and cysteine ligands can be compared here between Type 1 copper of blue-green Nir, the M182T mutant, and blue cupredoxins (*9*). A point mutation (M182T) was made at the methionine liganding position of the Type 1 copper. This single point mutation converted the Type 1 blue-green center to a blue Type 1 center and increased the redox potential from 247 to 354 mV (previous paper). Although much effort has been invested in understanding the structural, redox, and spectroscopic implications of point mutations at and near the Type 1 center in simpler azurins (*10*−*13*), we are unaware of any previous ENDOR study that has yet probed and compared the detailed covalent spin density changes accompanying such point mutations.

The catalytic Type 2 center has a more typical (inorganic) cupric EPR spectrum than Type 1; it has larger values of $g_{||}$ and $A_{||}$. This center has the tetrahedral copper environment shown in Figure 1 comprised of three histidine nitrogen ligands and, in the absence of nitrite, a water. In the presence of nitrite the crystallographic indication is that nitrite binds asymmetrically to the copper through its oxygen(s) (*2*). In the trimer of Type 2 His ligands His^{338} belongs to a different subunit from His^{166} and His^{131}. It may be significant from an electron-transfer standpoint that the His^{166} ligand of the Type 2 center is adjacent in sequence to the Cys^{167} ligand of the Type 1 center so that Type 1 and Type 2 copper are ~12 Å distant. We have also included the nonliganding His^{287} in Figure 1 since the homologue of His^{287} in Nir from *A. cycloclastes* is positioned to control nitrite binding to Type 2 copper even though His^{287} is itself not one of the histidine Type 2 copper ligands (*2, 14*). Our mutation (H287E) of His^{287} to Glu^{287} eliminated enzyme activity (prior paper). For the Type 2 center we wanted to detect intimate electronic spin density information of the catalytically important HOMO. Such spin density information is beyond the resolution of X-ray crystallography and only secondarily reflected in crystallographically detectable distance and bond angle changes. Such information includes the following: (1) Unpaired electron spin differences between ligands. (2) Small changes in covalent spin densities brought on by substrate binding that may correlate with substrate-induced redox change. (3) Mutation-induced perturbation to the exchangeable ligand binding site to explain the importance of His^{287} in the catalytic function of the protein.

Some ENDOR studies in the past have used technically easier, commercially available X-band (9 GHz) ENDOR, but for the paramagnetic environs of metal centers in proteins, it has been almost invariably found that proton features centered near the free proton frequency (12−14 MHz at X-band fields) overlap in a confusing way with strongly hyperfine coupled features of other nuclei like histidine nitrogens. Q-band ENDOR (34 GHz), which is done at ∼4-fold higher magnetic fields, shifted the proton features above 40 MHz while nitrogens, whose nuclear Zeeman interaction is small, remained below 30 MHz. An earlier X-band study on Nir was carried out with such a commercial Bruker X-band ENDOR system operating at higher temperatures, with RF frequency modulation, and in the absorption (χ'') mode (*15*). Such a system had its limitations: Its X-band nature caused nitrogen and proton features to overlap, and absorption conditions, higher temperature, and frequency modulation are not well suited for elucidating broad features with hyperfine couplings greater than several megahertz. As systematically reported from at least five Type 1 blue proteins, Q-band ENDOR carried out at pumped helium temperatures under dispersion conditions has proved its worth in separately resolving strongly hyperfine-coupled cysteine β protons and liganding histidine nitrogens (*9*). No strongly coupled, unique Type 1 features from either nitrogen or protons were reported from the previous X-band studies of Nir [which, in any case, was on a Nir derivative that had a blue, rather than a blue-green, Type 1 copper (*15, 16*)]. Building upon recently developed Q-band resonator technology (*17*) and on the development of a high-yield expression system for making native and mutant Nir, the present work provides explicit elucidation of the spin densities at Type 1 and Type 2 centers to correlate with functional and redox properties in both native and mutant forms of Nir.

METHODS AND MATERIALS

Methods. Q-band (34 GHz) ENDOR measurements were performed under dispersion (χ'), rapid passage conditions with a cryogenically tunable TE_{011} Q-band resonator recently developed for cryogenic pumped helium temperature EPR and ENDOR measurements (*17*). The Q-band head was contained within the metal Dewar tail of a helium immersion cryostat (Janis Research Company, Inc., Wilmington, MA) and was interfaced to an ER 051 QG-D Bruker Q-band bridge having a low-noise, but minimally tunable, Gunn diode source. Field modulation (100 kHz) and ENDOR RF were provided by posts located within the resonator. Typical modulation fields (calibrated by the modulation broadening of a narrow standard EPR signal) were 2 G ptp. The RF typically had a ptp amplitude of 1 G, and for some of the work was pulsed with a 10% (10 μs on and 90 μs off) duty cycle. Data were repetitively averaged with the EW software provided by Scientific Software Systems (Normal, IL), and total accumulation times were about 10 min/spectrum. For computing peak frequencies and hyperfine couplings, the frequencies of ENDOR features were corrected for shifts in the direction of the sweep. Preliminary X-band ENDOR was carried out with an older X-band system described in ref 18. Standard X-band EPR spectra are shown in the previous paper.

Materials. Nitrite reductase from *R. sphaeroides* 2.4.3 was overexpressed in *E. coli* according to the methods described in the previous paper. Samples were concentrated by Amicon or Microcon concentrators. The total concentration of copper as measured by double integration of the EPR spectrum with comparison to a standard cupric perchlorate sample (*19*) was approximately 500 μM total copper. The protonated samples were prepared in pH 7.1, 0.05 M sodium phosphate buffer. Deuterated samples were prepared by exchanging protein in aqueous buffer into deuterated buffer (0.1 M sodium phosphate, pD = 7.2), using a 10-mL Sephadex G25 spin column previously equilibrated in the same deuterated buffer. Q-band samples of approximately 50-μL volume were contained within a precision (Vitrodynamics, Rahway, NJ) 2.0-mm i.d., 2.4-mm o.d. sample tube.

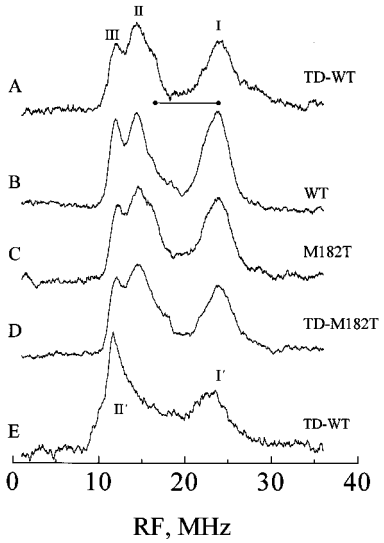

FIGURE 2: Q-band nitrogen ENDOR from Type 1 copper. Experimental conditions were T = 2.1 K, 100-kHz modulation = 2.3 G ptp, RF = 1.0 G ptp pulsed with 10% duty cycle, system time constant = 0.08 s, RF sweep rate = 3.5 MHz/s, microwave power = 0.3 μW, magnetic field = 12.02 kG at $g_x = 2.02$ for A−D and 11.12 kG at $g_z = 2.19$ for E, microwave frequency = 34.05 GHz. The ENDOR frequency range was 1−36 MHz. A was from Type 2 depleted wild-type enzyme; the bar is drawn with a length of $2^{14}\nu$ = 7.4 MHz. B was from wild-type enzyme. C was from M182T mutant. D was from the Type 2 depleted M182T mutant. E was from Type 2 depleted wild-type enzyme.

RESULTS

Type 1 Copper. The first-order expressions for ^{14}N ENDOR frequencies are

$$^{14}\nu_{\mathrm{ENDOR}}{}^{+} = |A/2 \pm 3P/2 + {}^{14}\nu| \quad (1)$$

$$^{14}\nu_{\mathrm{ENDOR}}{}^{-} = |\mathrm{A}/2 \pm 3P/2 - {}^{14}\nu| \quad (2)$$

where A is the hyperfine coupling, P the quadrupolar coupling, and $^{14}\nu$ (3.7 MHz at 12.0 kG, 3.3 MHz at 10.7 kG, and 0.8 MHz at 2.7 kG) is the ^{14}N nuclear Zeeman frequency. Particularly at 34 GHz, the ν^+ branch is often the only branch observed for ^{14}N (*20*). For Cu−His ligation the ^{14}N hyperfine interaction is generally dominated by isotropic Fermi coupling due to unpaired electron spin density in the nitrogen 2s orbital, and the elements of the quadrupolar tensor have typical magnitudes $|P| \leq 1.1$ MHz (*21*).

Spectra A, B, C, and D in Figure 2 from Type 2 depleted native, native, M182T, and Type 2 depleted M182T,

Table 1: ^{1}H and ^{14}N Hyperfine Couplings (MHz) Type 1

cysteine β protons			histidine nitrogen	
$A^{H1} = 20 \pm 0.2$ MHz	$\theta = 10°$	$\sigma_s = 21\%$	$A^{N1} = 39.2 \pm 0.4$ MHz	$f_s^a = 3.1\%$
$A^{H2} = 8.7 \pm 0.2$ MHz	$\theta = 130°$		$A^{N2} = 18.0 \pm 0.3$ MHz	$f_s^a = 1.5\%$

[a] f_s is the fraction of unpaired 2s electron spin.

respectively, were taken at the high-field EPR extremum ($g_x = 2.02$) dominated by the rhombic features of Type 1 copper where the observed ENDOR signal happened to be from Type 1 copper. At this extremum the spectra from the Type 2 depleted protein were identical to those of the nondepleted enzyme. The 7.4-MHz bar in Figure 2A shows where the Zeeman partner to feature I could plausibly lie. Features II (13.9 MHz) and III (11.5 MHz) are definitely not Zeeman partners of feature I (23.3 MHz). The implication is that the observed Q-band features are all ν^+ nitrogen features. As with other blue proteins (*9*), there were therefore two electronically distinguishable nitrogens, the first giving rise to feature I and the second giving rise to features II and III (or II′ at g_z). The frequencies of the nitrogen features from native (A and B) and from the M182T mutant (C and D) are remarkably similar. The Type 1 nitrogen features (not shown) from the H287E at the Type 2 center mutant were also similar to native Type 1. The nitrogen features I′ and II′ obtained at the $g_z = 2.19$ extremum (Figure 2E) from the Type 1 copper in the TD enzyme were similar in their frequencies to the nitrogen features observed at $g_x = 2.02$ (Figure 2A); thus the nitrogen hyperfine couplings are essentially isotropic, as expected when the major contribution is from a Fermi contact term. (See Table 1.) The decrease of about 1.5 MHz between the average frequency (12.7 MHz) of II and III and the frequency (11.2 MHz) of the single feature II′ is evidence for a small hyperfine anisotropy. The lack of splitting in II′ at $g_z = 2.19$ implies that the component of its nitrogen quadrupolar coupling is less than ~0.2 MHz; histidine nitrogen ENDOR spectra of Werst (*9*) obtained at g_z extrema from a number of blue proteins also showed no quadrupolar splittings. The direction for minimal quadrupolar coupling of imidazole nitrogen is normal to the plane of the imidazole in the π-bonding direction, as has been determined for both Cu-liganded histidine nitrogen (*21*) and heme iron-liganded histidine nitrogen (*22*). When there is **g**-tensor anisotropy ($g_z = 2.19$ vs $g_x = 2.02$), angle selection of different anisotropic elements of the quadupolar tensor at the respective low-field and high-field extrema is highly likely. Therefore it is possible that g_z is perpendicular to the histidine imidazole plane for feature II′. The 2.7-MHz splitting between features II and III at $g_x = 2.02$ is consistent with a larger $|P| \sim 0.9$ MHz quadrupolar component for the nitrogen belonging to these features, such as has been found in the histidine complexes of refs 21 and 22, either along the metal nitrogen bond or perpendicular to that bond in the plane of the imidazole, but not perpendicular to the imidazole plane.

Proton ENDOR frequencies, $^{p}\nu_{ENDOR}$, center to first order at the proton Larmor frequency, ν_p (>44 MHz for fields used at Q-band), and split away from the proton Larmor frequency by $\pm A/2$, the electron−proton hyperfine coupling, whence $^{p}\nu_{ENDOR} = |\nu_p \pm A/2|$. Figure 3 shows the strongly coupled proton features having $|A| = 20.0$ and 8.7 MHz from Type 1 copper of Nir. Spectra A (TD-native), B (native), C (M182T), and D (M182T-TD) in Figure 3 were taken at the high-field $g_x = 2.02$ extremum. The best-resolved features are from the ν^+ branch occurring above the free proton frequency, although with effort the ν^- branch could be seen, as shown in the inset. The proton ENDOR of the M182T mutant (Figure 3C,D) showed negligible difference in hyperfine splittings from Figure 3A,B. From Type 2 depleted enzyme for which there was never a possibility of overlapping Type 2 features, nearly identical proton features to those observed at $g_x = 2.02$ were also obtained at the $g_z = 2.19$ low-field extremum (Figure 3E), and so the proton couplings were indeed isotropic, as expected for the cysteine β protons. Features with splittings of order 20 MHz have been reported for other Type 1 blue proteins, while an 8.7-MHz coupling is smaller than generally reported [although stellacyanin showed such a proton hyperfine splitting that was not assigned (*9*)]. The feature with splitting of 8.7 MHz cannot be from a proton of Met^{182} since it is present in the M182T mutant. One would expect considerable anisotropic dipolar character from a proton on one of the imidazole rings, and the proton feature with a hyperfine coupling of 8.7 MHz does not show anisotropy.

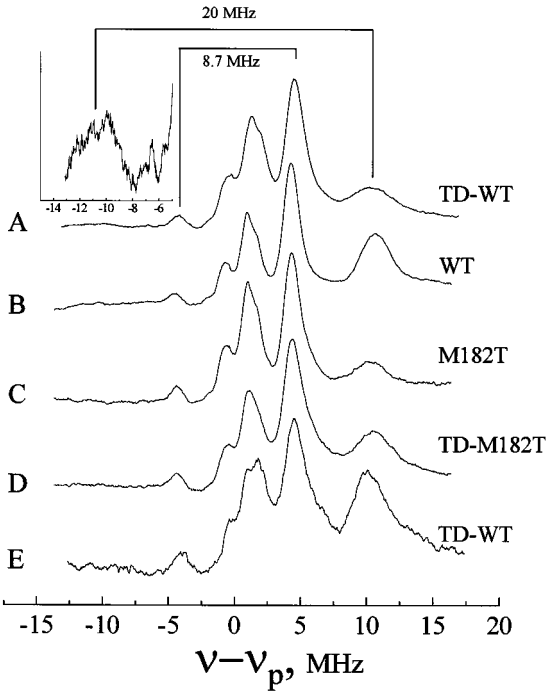

FIGURE 3: Q-band proton ENDOR from Type 1 copper. Experimental conditions were T = 2.1 K, 100-kHz modulation = 2.3 G ptp, RF = 1.0 G ptp. System time constant = 0.08 s, RF sweep rate = 3 MHz/s, microwave power = 0.3 μW, magnetic field = 12.02 kG at $g_x = 2.02$ for A−D and 11.12 kG at $g_z = 2.19$ for E, microwave frequency = 34.0 GHz. A was from Type 2 depleted wild-type enzyme; inset to show ν^- features has 20-fold higher gain. B was from wild-type enzyme. C was from the M182T mutant. D was from the Type 2 depleted M182T mutant. E was from Type 2 depleted wild-type enzyme. ENDOR frequency range was ± 15 MHz centered at the free proton NMR frequency, ν_p.

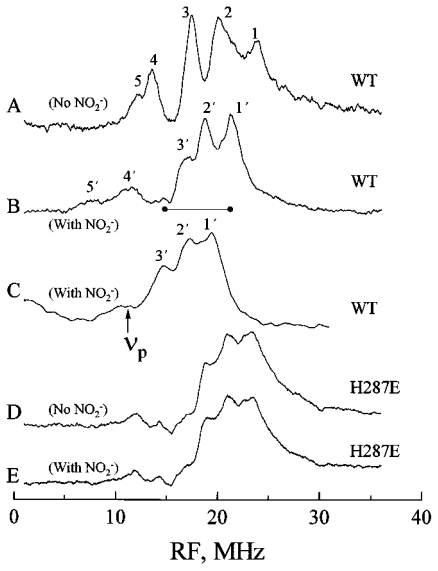

FIGURE 4: ENDOR spectra in the 1−35 MHz region primarily showing nitrogen features assigned to histidine nitrogens of Type 2 copper. Traces A, B, D, and E were Q-band ENDOR spectra obtained under the following conditions: T = 2.1 K, 100-kHz modulation = 2.3 G ptp, RF = ∼1 G ptp pulsed with 10% duty cycle, system time constant = 0.08 s, RF sweep rate = 3.5 MHz/s, microwave power = ∼0.3 μW, microwave frequency = 34.05 GHz, (A, 256 scans; B, 64 scans; D and E, 128 scans). Features 1, 2, 3, 4, and 5; 1′, 2′, 3′, 4′, and 5′ are assigned to histidines as discussed in text. Trace A is from wild-type Nir, no nitrite, H = 10.27 kG. Trace B is from wild-type Nir in the presence of 6 mM nitrite, H = 10.47 kG. Trace D is from the mutant H287E in the absence of nitrite and trace E in the presence of nitrite. Trace C, for comparison with trace B, was the X-band ENDOR spectrum from wild-type Nir containing 6 mM nitrite. The conditions for C were the following: T = 2.1 K, 100-kHz modulation = 3 G ptp, RF = ∼0.5 G ptp, system time constant = 0.08 s, RF sweep rate = 3.5 MHz/s, microwave power = ∼1 μW, magnetic field = 2.7 kG, microwave frequency = 9.169 GHz, 20 min data collection.

Type 2 Copper. Because Type 2 copper has larger $g_{||}$ and $Cu-A_{||}$ values than Type 1 copper, the ENDOR features from Type 2 copper are separable from overlapping Type 1 features for g values greater than ∼2.21 and fields less than ∼11 kG. Type 2 nitrogen hyperfine features were resolved in the 5−25 MHz region as shown in Figure 4. The Q-band ENDOR of native Nir in the absence of nitrite substrate (Figure 4A) revealed an intense set of three features (1, 2, and 3) at 23.4, 19.6, and 17.2 MHz, respectively; there were two weaker features (4 and 5) at 13.4 and 11.7 MHz. Nitrite substrate caused an overall change in electronic structure at the Type 2 copper. As shown in Figure 4B, 1′, 2′, and 3′ now occurred at 21.2, 18.5, and 16.5 MHz, and the lower-frequency features 4′ and 5′, now at 10.5 and 7.1 MHz, were split substantially more than their counterparts, 4 and 5. (Features from native Nir in the presence of nitrite are given primes.) A detailed comparison over a range of magnetic fields below 10.75 kG (i.e., above g = 2.26) showed that all of these nitrogen features in the presence of nitrite were consistently lower in frequency than their counterparts in the absence of nitrite. Therefore, the difference in overall nitrogen hyperfine coupling due to the presence or the absence of nitrite was independent of angle selection (*23*) brought on by any change in $Cu-A_{||}$ and $g_{||}$. Higher histidine nitrogen hyperfine frequencies for nitrite-free forms occurred at all fields below 10.75 kG so that even if there was site heterogeneity in nitrite-free, Type 2 EPR features (Figure 2, prior paper) the underlying histidine nitrogen ENDOR remained always at a higher frequency in the absence of nitrite. The X-band ENDOR spectrum of native Type 2 Nir with nitrite is shown in Figure 4C. There is more hyperfine information on strongly coupled nitrogens available from this low-temperature X-band dispersion ENDOR spectrum than reported from more standard X-band absorption ENDOR (*9*), but at X-band the 10−20-MHz range is still a frequency regime where nitrogen and proton features overlap. Without additional information (from Q-band ENDOR) it would have been difficult to judge whether the X-band ENDOR features in X-band Figure 4C are from nitrogens or protons; in addition Q-band resolves new low-frequency features 4, 5, 4′, and 5′. The features labeled 1′, 2′, and 3′ in Figure 4C are shifted by the 2.5-MHz difference in $^{14}\nu$ to 1′, 2′, and 3′ in the corresponding Q-band spectrum in Figure 4B. For H287E the nitrogen features did occur in roughly the same location found in the native protein, although they were generally broader, as shown in the spectrum in Figure 4D. Significantly, there were *no changes* in these features from H287E upon the introduction of nitrite, as shown in Figure 4E. The nitrogen ENDOR features from the nonmutated Type 2 center of M182T were similar to and showed the same behavior with nitrite addition as those of native Nir.

Nitrite binding markedly altered the electronic structure of the native Type 2 copper in Nir as shown by changed histidine nitrogen hyperfine couplings, proton couplings (below), and changes in $Cu-A_{||}$ copper hyperfine coupling, but we observed no ENDOR signature from nitrite itself, either as naturally abundant $^{14}NO_2^-$ or as isotopically enriched $^{15}NO_2^-$. In particular, there were no new features centering at the ^{15}N Larmor frequency when $^{15}NO_2^-$ was used.

Proton ENDOR features for the Type 2 copper were measured well out on the low-field ($M_I = +3/2$) $g_{||}$ extremum and are shown in the spectrum in Figure 5A for native Nir. It is clear (Figure 5B) that nitrite eliminated the features **a** and **a′** which have a splitting of 6.2 MHz. The corresponding features α and α′ from the H287E mutant (spectra E and F in Figure 5) had splittings at least as large as 6.2 MHz, and more significantly, there was no change in this large coupling in the presence of nitrite. The Type 2 proton features resolved from the M182T mutant also were similar to and showed the same behavior with nitrite addition as those of native Nir. As shown in spectra C and D in Figure 5 which were obtained in D_2O, we also looked to see which protons were exchangeable with solvent. In the well-resolved region of spectra C and D in Figure 5 *above* the free proton frequency, it was clear from a comparison of spectra A (H_2O) and C (D_2O) that the proton labeled **a** exchanged in the native nitrite-free protein, and there was *no evidence* for any other exchangeable protons upon comparison of spectra B (H_2O) and D (D_2O) in Figure 5 for the nitrite sample. (The corresponding feature α of the H287E also disappeared upon solvent deuteration.) In the presence of D_2O, as shown in Figure 5C,D, there was a passage or cross relaxation effect that partially diminished all weakly coupled proton features below ν_p. However, there was sufficient ENDOR intensity of features below ν_p for us to estimate that **a′** was indeed eliminated from the nitrite-free deuterated spectrum C in Figure 5 and that no exchangeable protons below ν_p were eliminated from the nitrite-containing deu-

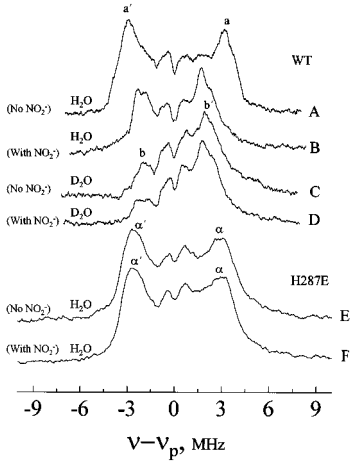

FIGURE 5: The proton ENDOR features from the Type 2 copper center. Spectra A, B, E, and F are from protein in protonated solvent; C and D are from protein in deuterated solvent: (A) wild type (protonated) in the absence of nitrite, $H = 10.27$ kG, (B) wild type (protonated) with 6 mM nitrite, $H = 10.42$ kG, (C) wild type (deuterated) in the absence of nitrite, $H = 10.32$ kG, (D) wild type (deuterated) with 6 mM nitrite, $H = 10.42$ kG, (E) the H287E mutant (protonated) in the absence of nitrite, $H = 10.27$ kG, and (F) the H287E mutant (protonated) in the presence of nitrite, $H = 10.27$ kG. Experimental conditions were $T = 2.1$ K, 100-kHz modulation = 1.2 G ptp, RF = 1.0 G ptp, pulsed with 10% duty cycle (10 μs on, 90 μs off) for spectra C, D, E, and F; system time constant = 0.04 s, RF sweep rate = 3.0 MHz/s, microwave power = 0.3 μW, microwave frequency = 34.05 GHz, (A, 200 scans; B, 128 scans; C, 400 scans; D, 512 scans; E, 32 scans; F, 32 scans). Features **a** and **a′** have a splitting of 6.2 MHz, α and α′ have a splitting of 5.9 MHz, and **b** and **b′** have a splitting of 4 MHz.

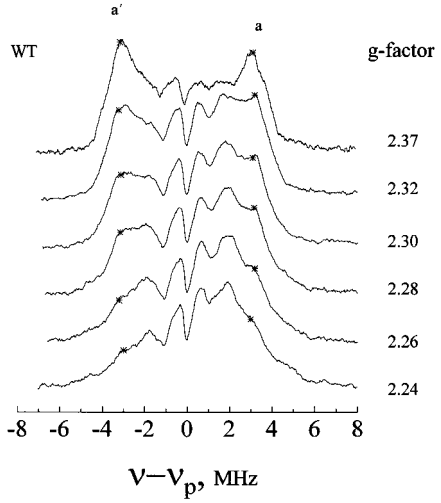

FIGURE 6: Proton ENDOR angle selection behavior versus *g* values of wild-type Nir in protonated solvent in the absence of nitrite. Note the behavior of the features **a** and **a′** which are exchangeable water features. The starred (*) features are the computed positions from angle-selected ENDOR of exchangeable water proton features predicted to have a maximum dipolar coupling of 6.4 MHz (A_{dip} = 3.2 MHz) and to lie at an angle (ω) of ~20° with respect to the $g_{||}$ direction.

terated spectrum D in Figure 5.[2] A small nonexchangeable hyperfine splitting ~4 MHz for the features **b** and **b′** was observed at $g_{||}$ in the nitrite-containing sample and in deuterated samples, and such splitting is consistent with that expected from imidazole protons on carbons adjacent to the liganding nitrogen (*24*). The X-band ENDOR study of Howes et al. (*15*) reported the existence of exchangeable protons having ~8 MHz hyperfine coupling; we find no evidence whatsoever for such protons. From the nitrite derivative no exchangeable protons were observed that had couplings ~6.2 MHz comparable to those observed from the aquo derivative. As shown in Figure 6A, we followed the spectroscopic details of outlying features **a** and **a′** from native Nir in protonated solvent as a function of the *g* value. It was clear that the hyperfine splittings of **a** and **a′** were maximal and best resolved over the *g* value range 2.37−2.30; in fact their splitting may be slightly larger at $g = 2.34$ and 2.32 than at 2.37. Their resolution diminished as the *g* value decreased, but their maximal splitting stayed at about 6.4 MHz until a *g* value of ~2.26 was reached.

DISCUSSION

Type 1 Center. Even though there was a blue-green to blue color change and a reduction potential increase brought on by the mutation M182T, the ENDOR frequencies (Figures 2 and 3) of native Nir and the M182T were identical. The proton and nitrogen ENDOR features are those respectively assigned to strongly coupled cysteine β protons and to histidine nitrogens (*8*, *9*). This is direct evidence that the electron spin density at the cysteine and histidine, that is, at the essential Type 1 ligands, is the same in the native Nir and the M182T mutant. There was also no change between native and M182T mutant in copper hyperfine couplings or *g* values (Figure 3, previous paper). A detailed spectroscopic/theoretical model of LaCroix et al. (*7*) has recently appeared with the goal of defining the electronic structural difference of the Type 1 site in Nir relative to the blue site of plastocyanin. Stronger ligation of the methionine ligand in Nir, evidenced by a shorter Met(S)−Cu bond than in plastocyanin, was deduced as the deciding factor in the electronic structural difference. Based on SCF-Xα-SW calculations, the important predictions of this model were a rotation of the $d_{x^2-y^2}$ orbital in Nir leading to a more intense ligand-to-metal 450-nm charge-transfer transition, a change in the covalent electronic overlap of the $d_{x^2-y^2}$ orbital with cysteine sulfur pπ orbitals, and a decrease in the electronic population on the cysteine sulfur in the spin-containing HOMO (Table 2, orbital 48a, ref 7) that would lead to lower spin density. It is true (see below) that the average hyperfine coupling to the two observed cysteine proton features of Nir is less than that observed for plastocyanin. However, there are predictions of the model which are inconsistent with our experiments.

The weaker threonine ligand in our M182T mutant definitely did lead to a conversion to a blue site (Figure 1, previous paper) and to an increased redox potential which happens to be similar to that of plastocyanin; nevertheless, by the same change in axial ligation, covalent spin densities in the critical HOMO were unaltered at the histidine and cysteine of M182T. If the model of ref 7 is correct, it is not obvious how a methionine-induced change in cysteine pπ−$d_{x^2-y^2}$ covalent overlap can be responsible for a change in optical charge-transfer transitions but can leave the electron spin density arising from pπ−$d_{x^2-y^2}$ overlap unchanged.[3] Our conclusion is that the deciding factor of histidine and cysteine

[2] Coupled relaxation pathways influence the proton ENDOR intensity (*20*), and these may involve cross-relaxation (spin diffusion) to bulk protons. For deuterated samples bulk protons are largely eliminated.

Table 2: ^{14}N Histidine Hyperfine Couplings (MHz), Type 2

wild-type without nitrite			wild-type with nitrite		
features	A^N (MHz)	f_s[a]	features	A^N (MHz)	f_s[a]
1, 2	36.7 ± 0.4	2.9	1′, 2′	33.1 ± 0.2	2.6
2, 3	30.5 ± 0.3	2.4	2′, 3′	28.4 ± 0.3	2.2
4, 5	18.8 ± 0.3	1.5	4', 5′	11 ± 0.8	0.9

[a] f_s is the fraction of unpaired 2s electron spin.

covalent differences between blue and blue-green Type 1 centers is not a different methionine ligation. Perhaps the determinant is the more subtle deciding factor of protein conformation (H-bonds, tertiary interactions, and strains as shown in Figure 1 of ref 25) that was not explicitly considered in the model of ref 7. Except for the single point mutation this protein conformation would be the same between wild-type Nir and its M182T mutant, but it differs in numerous aspects between plastocyanin and Nir.

Type 1 Nitrogen ENDOR Analysis. Taking the Type 1 nitrogen features of Figure 2 and Table 1 as ν^+ features, we estimate their respective average isotropic hyperfine couplings from $g = 2.02$ and $g_z = 2.19$ as 39.2 MHz (for I and I′) and 18 MHz (for II, II′ and III). The larger coupling is among the highest and the smaller coupling among the lowest of Type 1 histidine nitrogen couplings tabulated by Werst et al. (*9*) for five blue proteins (plastocyanin, azurin, stellacyanin, fungal laccase, and tree laccase). The implication is one of a marked difference in underlying unpaired electron spin density between His^{126} (or 95 in *A. cycloclastes*) and His^{177} (or 145 in *A. cycloclastes*). The 2.2 ratio of these couplings in Nir is larger than the ratio for any of the other reported blue proteins (*9*). Unpaired electron density in copper ligand orbitals reflects covalent overlap with the $d_{x^2-y^2}$ orbital that is sensitive to bond distances and bond angles. The His^{126}−Cu bond length and the His^{177}-Cu bond length are both 2.01 Å to within their standard deviation (*2*); however, the Met(S)^{182}−Cu−His (N)^{126} bond angle is 89° and the Met(S)^{182}−Cu−His(N)^{177} bond angle is 133° so that these angles differ from each other by 44°. Plastocyanin has identical histidine nitrogen couplings of 22 MHz (*9*), and its Met(S)−Cu−His(N) bond angles are both close to 90° and differ from each other by ∼13° (*5*). If the spin-containing $d_{x^2-y^2}$ orbital is perpendicular to the Met(S)−Cu bond, as experimentally inferred in plastocyanin from single-crystal elucidation of the g_z direction (*26*), then the His^{177} liganding nitrogen [corresponding to His^{145} in *A. cycloclastes*] would lie further out of the $x-y$ plane and would be less ideally located for optimal angular overlap of its pσ bond with the $d_{x^2-y^2}$ orbital.[4] The implication is that the large difference in spin densities between the two Type 1 histidine ligands of Nir reflects the respective Met(S)−Cu−His bond angle differences.

We next explicitly determined spin density on the Type 1 histidine nitrogens. A standard approach (*22*, *27*) was used to estimate from hyperfine coupling constants the covalent spin density on the histidine nitrogens. The majority of coupling to σ-bonded nitrogens is from Fermi contact interaction with the 2s electron in the nitrogen sp^2 σ-antibonding orbital.[5] The Fermi coupling to an electron with 2s character is

$$A_{\mathrm{FERMI}} = 16\pi g_n \beta_n \beta_e |\Psi_{o2s}|^2 f_s/(3h) \qquad (3)$$

where $|\Psi_{o2s}|^2$ is the square of the 2s wave function at the nitrogen nucleus [$=33.4 \times 10^{24}\mathrm{cm}^{-3}$ (*28*)], $g_n = 0.403$ is the ^{14}N nuclear g factor, and f_s is the fraction of an electron spin in a particular nitrogen 2s orbital. The percentages of unpaired 2s electrons predicted from Fermi couplings are listed in Table 1. The isotropic Fermi couplings of 39.2 and 18 MHz for the two Type 1 nitrogens of Nir corresponded to unpaired 2s electron spin densities of 3.1% and 1.5%, respectively, and a total 2s spin density of 4.6%. For plastocyanin the two histidine nitrogens (*9*) would each have 1.7% 2s electron spin density and a total 2s histidine spin density of 3.4%. The 2s electron spin density for the histidines of Nir is ∼35% higher than that on the histidines of plastocyanin. If both of the 2s contributions in Nir were to come from sp^2 orbitals having twice as much 2p as 2s character, then the total covalency associated with Type 1 histidine nitrogen orbitals of Nir would be 13.8% of an unpaired electron; a slightly different, more obviously empirical method [in which an isotropic coupling of 47 MHz corresponds to a total spin density of 10% (*9*, *27*) would predict 12.1% of an unpaired electron associated with Type 1 histidine nitrogens. Thus the experimentally measured nitrogen spin density in the 12−14% range for Type 1 copper in Nir is significantly twice as large as the histidine nitrogen spin covalency of 7% predicted by recent SCF-Xα-SW calculations to be in the Nir HOMO (*7*). The histidine ligation may play a more important role in the HOMO vis-à-vis cysteine than the Xα calculations (*7*) would have predicted. It is not clear if the Xα calculations predicted the observed electronic inequivalence of histidine hyperfine couplings.

Type 1 Cysteine β-Proton Hyperfine Analysis. The major hyperfine coupling mechanism for a cysteine β proton is hyperconjugation arising from spin in the adjacent sulfur pπ orbital. Calculations of Solomon and co-workers (*29*−*31*) for plastocyanin suggest that in the HOMO there is electron

[3] One might argue that the rotation of the $d_{x^2-y^2}$ hypothesized in ref 7 may still leave the same net covalent overlap with cysteine sulfur π orbitals in the antibonding, spin-containing HOMO but may alter the angular electronic overlap of $d_{x^2-y^2}$ with the two cysteine sulfur pπ orbitals in filled bonding orbitals that enter into the 600- and 450-nm optical charge-transfer transitions.

[4] It is not experimentally clear, since single-crystal EPR studies have yet to be done on the blue-green center of Nir, how its $d_{x^2-y^2}$ orbital points with respect to the Type 1 copper ligands. The SCF-Xα-SW calculations of ref 7 predicted a complex rotation of $d_{x^2-y^2}$ with respect to ligands.

[5] The hyperfine anisotropy between feature II′ and the average of features II and III in Figure 2 is approximately 3 MHz, and if this anisotropy is due to coupling with nitrogen 2p spin density, the 2p unpaired spin density would be approximately 2.1% [see eq 8 of ref 22] compared to a 2s spin density of 1.5%.

transfer between copper and cysteine sulfur. This transfer is due to overlap of the sulfur pπ orbital with the spin-containing copper $d_{x^2-y^2}$ orbital in a molecular orbital perpendicular to the Cu−S(Cys) bond and in a direction perpendicular to the Met(S)−Cu−S(Cys) plane. This molecular orbital accounts for considerable sulfur covalency in the HOMO and is a factor in the ligand-to-metal charge-transfer optical transition that leads to the Type 1 blue character. The model of ref 7 predicts that change in this sulfur−copper overlap due to a rotation of the $d_{x^2-y^2}$ orbital with respect to the Cu−S(Cys) bond would lead to the blue-green color of the Nir Type 1 site.

Since hyperconjugation is the critical electron spin transfer mechanism from sulfur pπ τo adjacent β protons, one can relate the observed β-proton coupling to the unpaired spin density in the sulfur pπ orbitals and to the dihedral angle, θ, that the S−C_β−H_β plane makes with respect to the direction of the spin-containing pπ orbital. The expression for couplings, A^{H1} and A^{H2}, to the two cysteine β protons, H_1 and H_2, is (*32*)

$$A^{H1} = B[\cos^2\theta]\sigma_s \quad \text{and} \quad A^{H2} = B[\cos^2(\theta - 120°)]\sigma_s \tag{4}$$

where B equals ∼ 100 MHz for a sulfur π orbital containing an entire electron spin; σ_s is the π spin density on the sulfur. Because of the $\cos^2\theta$ dependence in eq 4, there will be in principle two possible solutions, each having a pair of angles and a spin density, which satisfy the experimental values of A^{H1} and A^{H2}. To resolve the ambiguity over which set of θ, $\theta - 120°$, and σ_s is correct, one needs structural information on the Cu−S−C_β−H_β dihedral angles. Dihedral angles are readily obtained from the Protein Data Bank crystallographic coordinates of ref 2 by application of the SiGraphics Insight and Discover routines, but one needs insight on whether the sulfur pπ orbital normal to the S−C_β bond should be contained in the Cu−S−C_β plane or be perpendicular to the Cu−S−C_β plane. According to the picture of the Type 1 HOMO wave function developed for plastocyanin (*26*, *29*), the copper $d_{x^2-y^2}$ orbital strongly overlaps in an antibonding orbital with the sulfur π orbital which is *perpendicular* to the Cu−S−C_β plane. Therefore, in this picture the dihedral angles that are the required values of θ and $\theta - 120°$ are in fact the complements of the angles provided by the SiGraphics routine. These structurally predicted angles are $\theta = 150°$ and $(\theta - 120°) = 30°$, not ±60°; for $\theta = 150°$ the positive direction of the pπ orbital lies at 150° to the S−C_β−$H_{\beta 1}$ plane, and for $\theta - 120^o = 30°$ the positive direction of the pπ orbital lies at 30° to the S−C_β−$H_{\beta 2}$ plane.[6] $A^{H1} = 8.7$ MHz and $A^{H2} = 20$ MHz yielded either the set $\theta = 130°$, $\theta - 120° = 10°$, and $\sigma_s = 21\%$ or the set $\theta = 53°$, $\theta - 120° = -67°$, and $\sigma_s = 56\%$. The ENDOR-elucidated $\theta = 130°$, $\theta - 120° = 10°$, and $\sigma_s = 21\%$ is our preferred solution because it puts the dihedral planes only 20° away from their structurally predicted position; also $\sigma_s = 56\%$ is unrealistically large. A rationale for the difference between the structurally predicted (*2*) $\theta = 150°$ and $\theta - 120° = 30°$and the $\theta = 130°$ and $\theta - 120° = 10°$ is that the overlapping Cu $d_{x^2-y^2}$ orbital is rotated with respect to the Cu−S(Cys) bond. The 21% unpaired spin density is somewhat smaller, but comparable to, the 28% sulfur pπ character in the HOMO predicted by ref 7.

Type 2 Copper. We first point out important qualitative findings from histidine nitrogen couplings. For native Nir the most significant finding was that the entire ENDOR pattern from the liganding histidine nitrogens was shifted to lower frequency in the presence of nitrite (compare spectra A and B in Figure 4). The evidence that emerges is for decreased ligand covalency within the critical $d_{x^2-y^2}$ HOMO. It is not clear from X-ray crystallography if the changes in histidine bond lengths or copper−ligand bond angles upon nitrite binding are statistically significant (e.g., see Tables VII and IX of ref 2); EXAFS indicated an increase of slightly less than 0.1 Å in the average Type 2 histidine bond lengths upon nitrite binding (*14*). The evidence from ENDOR for changed electronic structure is unequivocal.

In the presence of nitrite all of the hyperfine couplings of corresponding features were lower (see Table 2) by at least ∼10% for features 1′, 2′, and 3′ and even more for 4′ and 5′. Hence, the binding of nitrite modulated the covalent interaction between the copper orbitals and histidine pσ orbitals. This decreased ligand covalency did not happen for H287E in the presence of nitrite and is an indication that the Type 2 center in this mutant is less sensitive to nitrite. For the native enzyme a nitrite-induced decrease in overall covalency of the spin-containing highest molecular orbital (HOMO) would imply less ligand field stabilization of the cupric Type 2 center (*33*). A decreased ligand (or crystal field) stabilization of the cupric state will make it easier to add an electron to the cupric Type 2 center to yield the cuprous, reduced Type 2 center and will in effect contribute to raising the redox potential of the Type 2 copper. In the course of redox titrations (adjacent paper) we estimated that the redox potential of the Type 2 center *in the absence of reducible nitrite substrate* was <200 mV. The redox potential of the native Type 1 center was ∼250 mV so that in the absence of nitrite the Type 2 center was not reduced. Therefore an increase in the redox potential of the Type 2 center when nitrite is bound is highly desirable for activity since an increase in the Type 2 redox potential would then enhance the likelihood of electron transfer from the Type 1 center to the Type 2 center.

Type 2 Nitrogen ENDOR Analysis. Since there are no higher-frequency nitrogen features than features 1, 2, and 3 for substrate-free enzyme (Figure 4A) and 1′, 2′, and 3′ for nitrite-bound enzyme (Figure 4B), these features must be ν^+ features. [The comparison of features 1′, 2′, and 3′ at Q-band (spectrum B in Figure 4) versus 1′, 2′, and 3′ at X-band (spectrum C in Figure 4) is highly consistent with these features being the ν^+ features which are shifted upward at Q-band by an expected $\Delta^{14}\nu = 3.3 - 0.8 = 2.5$ MHz.] We next provide an assignment of nitrogen features to show significant electron difference of one of the Type 2 histidine

[6] When we applied the same approach to the plastocyanin cysteine proton data as Werst et al. (*9*). We obtained ENDOR-elucidated dihedral angles of $\theta = 137°$ and $\theta - 120° = 17°$ taken with respect to the π orbital and $\sigma_s = 30\%$ of an unpaired sulfur π electron in the HOMO, compared with 35% predicted by Xα theory. Werst et al. (*9*) made the alternative choice for the larger set of dihedral angles at ∼±60°. In the absence of further corrections to our eq 4, such a choice would give unrealistically large sulfur π spin density > 50%. Werst et al. (*9*) included an additional constant term besides the $\cos^2\theta$ term when they related β proton hyperfine coupling to pπ spin density, and the upshot was that their cysteine sulfur pπ spin density reported for plastocyanin was 44%.

nitrogen ligands from the other two. The assignment is most straightforwardly done for the Nir in the presence of nitrite (Figure 4B). At fields on the order of 10.3 kG the splitting between corresponding ν^+ and ν^- Zeeman partners would be $2^{14}\nu$ = 6.4 MHz, and a line of length 6.4 MHz is accordingly provided in Figure 4. In Spectrum B in Figure 4, only 3′ and 4′ could be Zeeman partners. It is unlikely that some nitrogens (1′, 2′, and 5′) of a pattern would have no Zeeman partners while spectrally similar 3′ and 4′ would. Our conclusion is that all Type 2 nitrogen features are ν^+ features for Nir-nitrite-containing samples and that the features 4′ and 5′ are from a weakly hyperfine-coupled nitrogen electronically different from the strongly coupled nitrogens which cause features 1′, 2′, and 3′. On the basis of the overall similarity of the entire pattern 1, 2, 3, 4, and 5 (spectrum A in Figure 4) to 1′, 2′, 3′, 4′, and 5′ (spectrum B in Figure 4), we assign features 4 and 5 to a nitrogen markedly distinct from the nitrogens causing features 1, 2, and 3, just as we assigned 4′ and 5′ to a nitrogen markedly distinct from 1′, 2′, and 3′.

Since 1, 2, and 3 and 1′, 2′, and 3′ present three features, they must represent at least two histidine nitrogens. A consistent interpretation[7] is to have features 1−2 and 2−3 for the native nitrite free enzyme represent two slightly inequivalent nitrogens with respective hyperfine couplings (*A*) of 36.7 and 30.5 MHz and quadrupolar couplings |*P*| of 1.3 and 0.8 MHz. The features 1′ and 2′ and 2′ and 3′ from Nir in the presence of nitrite would correspondingly have respective hyperfine coupling of 33.1 and 28.4 MHz and quadrupolar couplings |*P*| of 0.9 and 0.7 MHz. All of these hyperfine couplings are consistent with the ∼35-MHz couplings seen from copper imidazole (*24*) and Type 2 copper in superoxide dismutase (*34*). The features 4 and 5 from the nitrite-free Nir would then have a smaller hyperfine coupling of A = 18.8 MHz, $|P|$ = 0.6 MHz; the features 4′ and 5′ would have A = 11 MHz, $|P|$ = 1.1 MHz. A difference of 42 versus 28 MHz was reported between histidine nitrogen ligands of the Cu^{II} occupying the Zn^{II} site in $(Ag^{II})_2(Cu^{II})_2$SOD (*35*), but the difference in nitrogen hyperfine couplings observed here is larger than that reported for any other Type 2 copper center.

Whether or not nitrite is bound, we conclude that there are two strongly hyperfine-coupled histidine nitrogens and one weakly coupled histidine nitrogen at the Type 2 copper. [We are definitely observing more than one nitrogen, in contrast to the previous "provisionally assigned" case based on ENDOR features from the wild-type enzyme having a ∼3:1 signal-to-noise ratio (*15*).] The structures provided by ref 2 suggest flexibility of the Cu−His^{338} bond and possibly a reason for a difference of His^{338} nitrogen hyperfine coupling from His^{131} and His^{166}. The Cu−N bond length of His^{338} ligand (His^{306}, *A. cycloclastes*), which is located on the different (B) subunit, is about 0.2 Å longer than the Cu−N bonds to His^{131} (His^{100}, *A. cycloclastes*) and His^{166} (His^{135}, *A. cycloclastes*) located on the A subunit in the crystal form at low pH. The bond to His^{338} but becomes approximately equal to the other two in the crystal form studied at pH 6.8 (*2*). Histidine nitrogen inequivalence brought on by the protein may augment the natural tendency for a Jahn−Teller distortion of the cupric trigonal site symmetry that would foster electronic equivalence of histidine nitrogens. Next, not only is the hyperfine coupling to the more weakly coupled nitrogen significantly decreased in the presence of nitrite but also its quadrupolar coupling is increased. The implication is that binding of nitrite alters the local conformation at the Type 2 center, where the evidence for the alteration is greatest at the histidine that gives rise to the lower-frequency ENDOR features (4 and 5 versus 4′ and 5′).

The majority of hyperfine coupling to Type 2 histidine nitrogens (*21, 34*) is from Fermi contact interaction with the 2s contribution in the nitrogen sp^2 σ-antibonding orbital. Using the standard eq 3 approach, we predict for native, nitrite-free Type 2 copper in Nir that the unpaired 2s electron spin density is 2.9% and 2.4% for the two more strongly coupled nitrogens and 1.5% for the more weakly coupled nitrogen. The difference between the former two more strongly coupled nitrogens and the latter more weakly coupled protons is definitive. If all of these 2s contributions come from sp^2 orbitals having twice as much 2p as 2s character, then the total contribution from the three Type 2 histidine nitrogen orbitals is ∼20% of an unpaired electron. We would thus expect ∼80% of an unpaired electron to be located on the copper. The corresponding, diminished percentage of unpaired electron in the presence of nitrite is ∼17%.

One must be careful of overinterpreting negative results, but the absence of any $^{15}NO_2^-$ ENDOR feature, even a weak and poorly resolved one, does imply very weak hyperfine coupling to the nitrogen of nitrite. A combination of reasons may explain why the nitrogen of the nitrite does not show hyperfine structure. First, according to Adman et al. (*2*), the bonding to copper occurs through the oxygen(s) of the NO_2^- rather than the nitrogen. Second, the binding to nitrite, however it may happen, is evidently axial and orthogonal with respect to the d orbital ($d_{x^2-y^2}$) that contains electron spin. Third, the highest filled orbital of NO_2^- (by itself and independent of bonding to copper) is a nonbonding orbital having electron density on its oxygens but not on its nitrogen, and this is the orbital that would most likely partake in a covalent bond to copper via its oxygens. In model Cu(II) nitrite complexes ESEEM indicates hyperfine coupling to nitrite if it is a planar ligand within the $d_{x^2-y^2}$ plane (*36*), but in the case of mixed valence hemocyanin where nitrite is an axial ligand there was no resolved hyperfine coupling to it (*37*).

Type 2 Exchangeable Proton ENDOR Analysis. For protons which are sufficiently distant from the cupric ion and oriented so that little covalent spin density arrives on them, the dipolar hyperfine coupling, A_D, will be distance

[7] The splittings between features 1 and 2, 2 and 3, 1′ and 2′, 2′ and 3′ of Figure 4 are respectively 3.8, 2.4, 2.7, and 2.0 MHz, and such splittings yield values of |*P*| in the 0.5−1.3-MHz range; such splittings are consistent with quadrupolar splittings of copper-liganded histidine ^{14}N as observed in the imidazole plane (*22*). The ∼5-MHz splitting between features 1 and 3 or 1′ and 3′ predicts a ∼1.7-MHz value for |*P*| that is outside the quadrupolar range for histidine (*22*). Thus the predicted and tabulated hyperfine and quadrupolar couplings are the following: for features 1−2, A = 36.7 MHz, |*P*| = 1.3 MHz; for 2−3, A = 30.5 MHz, |*P*| = 0.8 MHz; for 1′−2′, A = 33.1 MHz, |*P*| = 0.9; for 2′−3′, A = 28.4 MHz, |*P*| = 0.7. For completeness, there are other slightly different interpretations of these features which still would predict two slightly inequivalent nitrogens. For example, 2 and 3 could have A = 30.5 MHz, |*P*| = 0.8 MHz and 1 (by itself) have A = 40.5 MHz and |*P*| ≈ 0; 2′ and 3′ could have A = 28.4 MHz, |*P*| = 0.7 MHz and 1′ (by itself) have A = 35.8 and |*P*| ≈ 0.

and angle-dependent.

$$A_D = \{f_{Cu} g_e g_n \beta_e \beta_n / hR^3\}(3\cos^2\omega - 1) = A_{dip}(3\cos^2\omega - 1) \quad (5)$$

where f_{Cu} is the fraction of an unpaired electron on the copper, g_e is the electronic g value, and g_n is the nuclear g value (= 5.585 for a proton). R is the copper−proton distance, and ω is the angle between the vector **R** and the external magnetic field. The overall dipolar Hamiltonian will be axial with respect to the **R** direction. In the simplest case where the $g_{||}$ tensor component is collinear with the proton−copper vector, the principal maximal proton hyperfine coupling ($A_{||}$) will be $2f_{Cu}g_{||}g_n\beta_e\beta_n/(hR^3)$, and when $f_{Cu} = 0.8$, $g_e = g_{||} = 2.34$, $A_{dip} = 3.2$ MHz, and $A_D = 6.4$ MHz, the predicted distance will be 2.85 Å. The principal axis of dipolar coupling need not be collinear with the **g**-tensor axes, and in frozen solution angle selection determines the position and resolution of ENDOR features. Hoffman and Gurbiel (*23*) devised a formulation for rapidly simulating polycrystalline ENDOR frequency patterns for systems such as Type 2 copper which have an axial g tensor and axial copper (^{63}Cu/^{65}Cu) nuclear hyperfine coupling. This formulation does not depend on a detailed simulation of ENDOR line shapes, and from it one can infer the magnitude of A_{dip} (and therefore R) and the angular orientation (ω) of the proton with respect to the $g_{||}$ axis. There will be subsets of spectra corresponding to each copper nuclear spin state, $M_I = {}^3/_2, {}^1/_2, -{}^1/_2, -{}^3/_2$. The g-value range over which the maximal hyperfine coupling, $A_D = 2A_{dip}$, is observed depends on the value of ω, and the exact value of measured ENDOR hyperfine splitting at the lowest field ($M_I = {}^3/_2$) EPR extremum provides, if it is less than $2A_{dip}$, evidence for $\omega \neq 0$. There are additional ENDOR features predicted by the theory of Hoffman and Gurbiel (*23*) besides the outlying ones, but realistically, these will be obscured in a protein by an abundance of other weakly coupled protons. In Figure 6 we show the predicted (starred) positions of the maximally split outlying features for the case where $A_{dip} = 3.2$ MHz and $\omega = 20°$. In the supplementary Figure S-1 we provide the detailed prediction of proton ENDOR frequencies versus g values from angle selected theory (*23*) for off-axis water protons where $\omega = 0°$, 10°, or 20°. In the Supporting Information, Figure S-2, we show patterns of proton frequencies calculated for $\omega = 0°$, 10°, 15°, 20°, and 30°. A fit to proton ENDOR features, which was realistically to the outlying features, was best obtained with ω in the 15−20° range. This fit predicted the range of g values (2.32−2.26) over which the maximal hyperfine splittings of 6.4 MHz were observed, and it predicted the slight diminishment of the splitting of these outlying features at the extreme minimal field where $g = 2.37$. Since there are several close-lying predicted features with splittings only slightly less than the maximal 6.4 MHz splitting in the g-value range 2.24−2.28, this overlay of predicted frequencies also provides an explanation for the shoulders extending inward from the two outlying proton features. The predicted distance to water protons from Adman et al. (*2*) was 2.85 and 2.7 Å, and starting with crystallographically located water oxygen (*2*), we would estimate that the off-axis angle should be about 16° as computed from the known Copper−water oxygen distance, from a water O−H distance of 1 Å, and from an H−O−H bond angle of 104°.

The proton couplings (Figure 5E,F) measured on the H287E mutant showed that the replacement of His^{287} by glutamate altered the binding site for nitrite sufficiently that water protons still remained liganded to the Type 2 copper. Since the nearest nitrogen of His^{287} to copper is still ∼4 Å from the copper, it is unlikely that the glutamate carboxylate group will directly bind to the copper. The carboxylate may repel nitrite and additionally stabilize the water by hydrogen bonding to it, but it has not replaced the axial water ligand. The ENDOR results on H287E dramatically reveal the insensitivity of its Type 2 axial ligation site to nitrite (Figure 5, E vs F) and lack of response of its histidine ligand hyperfine coupling to nitrite (Figure 4, D vs E). The ENDOR study of the H287E mutation, which does not remove the Type 2 center and is not a mutation of a direct His ligand to the Type 2 center, provides insight into the role of His^{287} in altering the Type 2 site structure.

CONCLUSIONS

Copper Nir contains a Type 1 blue-green copper (having two histidines, a cysteine, and a methionine ligand) which has a redox function and a Type 2 catalytic copper (having three histidine ligands) where nitrite reduction occurs. The enzyme studied is from a denitrifying variant of *R. sphaeroides* overexpressed in *E. coli.* ENDOR results were correlated with functional measures of activity and reduction potential and with spectroscopic results presented in the previous paper. We investigated native enzyme and two mutants, M182T having a Met → Thr replacement of the Type 1 Met ligand and H287E having a His → Glu replacement of a nonliganding His which markedly altered substrate binding at the Type 2 center. Q-band electron nuclear double resonance (ENDOR) probed the ligand hyperfine couplings and spin densities at both centers. ENDOR of the native blue-green Type 1 center showed ∼2-fold electronic spin inequivalence of the two His ligands. There was ∼21% electron spin delocalization to the Cys pπ sulfur, less than with other blue proteins.[6] The M182T mutant at the Type 1 center had a marked change in its optical absorption (blue instead of blue-green), an increase in redox potential, and a diminished activity. Surprisingly, the electron spin densities at the His and Cys ligands of M182T, ligands common to all Type 1 blue proteins, were unchanged from those in the native enzyme. All three His ligands of the Type 2 center contributed nitrogen hyperfine couplings, but as an indication of electronic distortion at the Type 2 Cu, one of the couplings was ∼2-fold less than the other two. Binding of nitrite at Type 2 copper induced a decrease in all His ligand hyperfine couplings, implying a decrease of covalent interaction with copper; such a change may correlate with a concomitant increase in the redox potential of the Type 2 center when nitrite is bound. Nitrite substrate eliminated exchangeable protons assigned to a water ligand. His^{287} sits close enough to the Type 2 center to perturb nitrite binding, and the H287E mutant showed no nitrite-induced electronic structural change and no nitrite-induced loss of water protons, and significantly, the H287E mutant had its enzymatic activity reduced by several orders of magnitude.

ACKNOWLEDGMENT

C.P.S. is grateful to Professors Jan Rydström, Tore Vänngård, and Bo Malmström for providing facilities at the Lundberg Laboratory, Göteborg University, in which preliminary functional and EPR studies on Nir took place in 1995. We appreciate conversations on Nir with Drs. Bengt Reinhammar and Örjan Hansson. We appreciate the advice and help of Dr. Susan Baxter, Wadsworth Center NMR Facility, New York State Department of Health, in the deuteration of small Nir samples.

SUPPORTING INFORMATION AVAILABLE

Figure 1-S which provides the detailed prediction of proton ENDOR frequencies versus *g* values from the angle-selected theory (*23*) for off-axis water protons where $\omega = 0°$, 10°, or 20° and Figures S-2 parts A, B, and C which respectively provide an overlay of angle-selected proton ENDOR from Figure 6 with all predicted proton ENDOR frequencies from the angle-selected theory of Hoffman and Gurbiel (*23*) for an off-axis water proton having an off-axis angle ω of 0°, 10°, 15°, 20°, and 30° (6 pages). Ordering information is given on any current masthead page.

REFERENCES

1. Godden, J. W., Turley, S., Teller, D. C., Adman, E. T., Liu, M. Y., Payne, W. J., and LeGall, J. (1991) *Science 253*, 438−442.
2. Adman, E. T., Godden, J. W., and Turley, S. (1995) *J. Biol. Chem. 270*, 27458−27474.
3. Murphy, M. E. P., Turley, S., Kukimoto, M., Nishiyama, M., Horinouchi, J., Sasaki, H., Tanokura, M., and Adman, E. T. (1995) *Biochemistry 34*, 12107−12117.
4. Tosques, I. E., Kwiatkowski, A. V., Shi, J., and Shapleigh, J. P. (1997) *J. Bacteriol. 179*, 1090−1095.
5. Guss, J. M., Bartunik, H. D., and Freeman, H. C. (1992) *Acta Crystallogr., Sect. B 48*, 790−807.
6. Norris, G. E., Anderson, B. F., and Baker, E. N. (1986) *J. Am. Chem. Soc. 108*, 2784−2785.
7. LaCroix, L. B., Shadle, S. E., Wang, Y., Averill, B. A., Hedman, B., Hodgson, K. O., and Solomon, E. I. (1996) *J. Am. Chem. Soc. 118*, 7755−7768.
8. Roberts, J. E., Cline, J. F., Lum, V., Freeman, H., Gray, H. B., Peisach, J., Reinhammar, B., and Hoffman, B. M. (1984) *J. Am. Chem. Soc. 106*, 5324−5330.
9. Werst, M. M., Davoust, C. E., and Hoffman, B. M. (1991) *J. Am. Chem. Soc. 113*, 1533−1538.
10. Karlsson, B. G., Nordling, M., Pascher, T., Tsai, L., Sjölin, L., and Lundberg, L. G. (1991) *Protein Eng. 4*, 343−349.
11. den Blaauwen, T., van de Kamp, M., and Canters, G. W. (1991) *J. Am. Chem. Soc. 113*, 5050−5052.
12. Andrew, C. R., Yeom, H., Valentine, J. S., Karlsson, B. G., Bonander, N., van Pouderoyen, G., Canters, G. W., Loehr, T. M., and Sanders-Loehr, J. (1994) *J. Am. Chem. Soc. 116*, 11489−11498.
13. Murphy, L. M., Strange, R. W., Karlsson, B. G., Lundberg, L. G., Pascher, T., Reinhammar, B., and Hasnain, S. S. (1993) *Biochemistry 32*, 1965−1975.
14. Strange, R. W., Dodd, F. E., Abraham, Z. H. L., Grossman, J. G., Brüser, T., Eady, R. R., Smith, B. E., and Hasnain, S. S. (1995) *Nat. Struct. Biol. 2*, 287−292.
15. Howes, B. D., Abraham, Z. H. L., Lowe, D. J., Brüser, T., Eady, R. R., and Smith, B. E. (1994) *Biochemistry 33*, 3171−3177.
16. Abraham, Z. H. L., Lowe, D. J., and Smith, B. E. (1993) *Biochem. J. 295*, 587−593.
17. Sienkiewicz, A., Smith, B. G., Veselov, A., and Scholes, C. P. (1996) *Rev. Sci. Instrum. 67*, 2134−2138.
18. Scholes, C. P., Falkowski, K. M., Chen, S., and Bank, J. (1986) *J. Am. Chem. Soc. 108*, 1660−1671.
19. Aasa, R., and Vänngård, T. (1975) *J. Magn. Reson. 19*, 308−315.
20. Hoffman, B. M., DeRose, V. J., Doan, P. E., Gurbiel, R. J., Houseman, A. L. P., and Telser, J. (1993) EMR of Paramagnetic Molecules, in *Biological Magnetic Resonance* (Berliner, L. J., and Reuben, J., Eds.) Vol. 13, Plenum Press, New York.
21. McDowell, C. A., Naito, A., Sastry, D. L., Cui, Y. U., Sha, K., and Yu, S. X. (1989) *J. Mol. Struct. 195*, 361−381.
22. Scholes, C. P., Lapidot, A., Mascarenhas, R., Inubushi, T., Isaacson, R. A., and Feher, G. (1982) *J. Am. Chem. Soc. 104*, 2724−2735.
23. Hoffman, B. M., and Gurbiel, R. J. (1989) *J. Magn. Reson. 82*, 309−317.
24. Van Camp, H. L., Sands, R. H., and Fee, J. A. (1981) *J. Chem. Phys. 75*, 2098−2107.
25. Adman, E. T. (1991) in *Advances in Protein Chemistry* (Anfinsen, C. B., Richards, F. M., Edsall, J. T., and Eisenberg, D. S., Eds.) Vol. 42, pp 145−197, Academic Press, San Diego.
26. Penfield, K. W., Gay, R. R., Himmelwright, R. S., Eickman, N. C., Norris, V. A., Freeman, H. C., and Solomon, E. I. (1981) *J. Am. Chem. Soc. 103*, 4382−4388.
27. Brown, T. G., and Hoffman, B. M. (1980) *Mol. Phys. 39*, 1073−1109.
28. Hartree, D. R., and Hartree, W. (1949) *Proc. R. Soc. London, Ser. A. 193*, 299−304.
29. Penfield, K. W., Gewirth, A. A., and Solomon, E. I. (1985) *J. Am. Chem. Soc. 107*, 4519−4529.
30. Gewirth, A. A., Cohen, S. L., Schugar, H. J., and Solomon, E. I. (1987) *Inorg. Chem. 26*, 1133−1146.
31. Gewirth, A. A., and Solomon, E. I. (1988) *J. Am. Chem. Soc. 110*, 3811−3819.
32. Gordy, W. (1980) *Theory and Applications of Electron Spin Resonance*; Wiley, New York.
33. Huheey, J. E., Keiter, E. A., and Keiter, R. L. (1993) *Inorganic Chemistry: Principles of Structure and Reactivity*, 4th ed., Chapter 11, pp 387−471, Harper-Collins.
34. Van Camp, H. L., Sands, R. H., and Fee, J. A. (1982) *Biochim. Biophys. Acta 704*, 75−89.
35. Gurbiel, R. J., Peoples, R., Doan, P. E., Cline, J. F., McCracken, J., Peisach, J., Hoffman, B. M., and Valentine, J. S. (1993) *Inorg. Chem. 32*, 1813−1819.
36. Jiang, F., Conry, R. R., Bubacco, L., Tyeklar, Z., Jacobson, R., Karlin, K. D., and Peisach, J. (1993) *J. Am. Chem. Soc. 115*, 2093−2102.
37. Bubacco, L., Magliozzo, R. S., Wirt, M. D., Beltramini, M., Salvato, B., and Peisach, J. (1995) *Biochemistry 34*, 1524−1533.

BI971604R